Structural Effects on the High Temperature Adsorption of CO_2 on a Synthetic Hydrotalcite

Nick D. Hutson*

National Risk Management Research Laboratory, U. S. Environmental Protection Agency, 109 T. W. Alexander Drive (E−305−01), Research Triangle Park, North Carolina 27711

Scott A. Speakman and E. Andrew Payzant

High-Temperature Materials Laboratory, Oak Ridge National Laboratory, Bethel Valley Road, P.O. Box 2008, Oak Ridge, Tennessee 37831

Received April 26, 2004. Revised Manuscript Received July 15, 2004

Hydrotalcite-like compounds (HTlcs) are solid sorbents that may potentially be used for high-temperature separation and capture of CO_2. The high-temperature adsorption of CO_2 on Mg−Al−CO_3 HTlc is affected by structural changes that take place upon heating of the material. The structural changes of a synthetic HTlc upon heating to 200 and 400 °C in a vacuum were characterized using various analytical techniques. These structural changes were then related to observed behavior with respect to the physisorption and chemisorption of CO_2 at 200 °C. Upon heating to 200 °C, the material retains its layered structure, though the interlayer spacing is decreased by ∼0.6 Å due to loss of interlayer water. Chemisorption of CO_2 at 200 °C represents more than half of the total adsorption capacity (at 107 kPa) due to increased availability of the framework Mg^{2+} cation and the subsequent formation of $MgCO_3$. There is no significant increase of surface area or pore volume after heating to 200 °C. Upon heating to 400 °C the CO_3^{2-} in the interlayer is decomposed and the material is completely dehydrated and partially dehydroxylated. The resulting amorphous 3-D structure with increased surface area and pore volume and decreased availability of the Mg^{2+} cation favors physisorption over chemisorption for these samples. An increased understanding of structure−property relationships will help in the further development of HTlcs as viable CO_2 solid sorbents.

Introduction

Increases in the atmospheric concentrations of gases such as methane (CH_4), nitrous oxide (N_2O), and, especially, carbon dioxide (CO_2) have enhanced the heat-trapping capability of the earth's atmosphere via the greenhouse effect. There are known ways to manage the emission of greenhouse gases. Increases in the efficiency of energy use are largely responsible for reduction of U.S. greenhouse gas intensity (the amount of greenhouse gases emitted in relation to economic growth) in the past 10 years. Carbon emissions may also be reduced by increasing the use of carbon-free or low-carbon energy sources (e.g., nuclear, biomass, solar, wind). A relatively new concept for the control of carbon emissions is that of carbon sequestration. In this option, carbon dioxide is captured and securely stored for long-term sequestration.

The costs of separation and capture, including compression, are estimated to make up about three-fourths of the total costs of ocean or geologic sequestration.[1] Currently, the most likely options for CO_2 separation and capture are (1) chemical and physical *ab*sorption, (2) physical and chemical *ad*sorption, (3) low-temperature distillation, (4) gas separation using membranes, and (5) mineralization. Among these, physical absorption using amine solvents is the only technology that is currently deployed commercially for CO_2 capture. However, there is a significant energy penalty associated with this technology from the heat required to regenerate the solvent (though some recent improvements have lessened this penalty). The goals of the carbon sequestration program are for technologies that result in <10% increase in the cost of energy for direct capture/sequestration and <$10 per metric ton of CO_2 that is indirectly sequestered.[2]

Selective adsorption has been identified as one of the ways to prevent the emission of CO_2 from fossil-fueled power plants and other sources. Pressure, vacuum, and temperature swing adsorption (PSA, VSA, and TSA, respectively) are proven technologies that are commonly used for many gas separations[3] and have been proposed for CO_2 separation and capture.[4−8] In the PSA opera-

* To whom correspondence should be addressed. Phone: (919) 541-2968. E-mail: hutson.nick@epa.gov.

(1) Reichle, D.; et al. *Carbon Sequestration Research and Development*; Office of Science, Office of Fossil Energy, U.S. Department of Energy, 1999.

(2) National Energy Technology Laboratory (NETL), *Carbon Sequestration Technology Road Map, Pathways to Sustainable Use of Fossil Energy*; U.S. Department of Energy, Office of Fossil Energy, 2003.

(3) Yang, R. T. *Gas Separation by Adsorption Processes*; Imperial College Press: London, UK, 1997.

10.1021/cm040060u CCC: $27.50
Published on Web 09/21/2004

tion, gases are selectively adsorbed at high pressure, isolated, and then desorbed by reducing the pressure. VSA is a simple variant of PSA, with a vacuum desorption cycle. In the TSA operation, the gases are adsorbed at lower temperature and desorbed by heating the sorbent bed. Recently, new adsorption cycles have been proposed. In these novel systems, enriching reflux and dual reflux PSA cycles are used in lieu of the traditional stripping reflux cycles that severely limit the enrichment of the heavy component.[9,10]

Many naturally occurring and synthetic materials have a high adsorption capacity for CO_2. An International Energy Agency (IEA) study evaluated CO_2 separation and capture using both PSA and TSA operational modes and employing 13X zeolite as the sorbent. The IEA report[11] concluded that PSA and TSA technologies are not economically attractive for the gas- and coal-fired power systems included in that study. This conclusion has led many to extrapolate the findings and to conclude that adsorption systems are not applicable for CO_2 separation and capture. This, however, is not necessarily true. It is true that the most commonly studied adsorbents (zeolites and activated carbons) suffer from low capacity at elevated temperatures and are thus limited to operation at lower temperatures. It is also true that the viability of an adsorptive separation process is clearly linked to the applicability of the sorbent. It follows then that, in order for adsorption technologies to be effective and viable for separation and capture of CO_2, new sorbents must be developed and tested. New sorbents are needed that have (1) high selectivity and adsorption capacity for CO_2 at elevated temperatures, (2) adequate adsorption/desorption kinetics for CO_2 at operating temperatures, (3) stable CO_2 capacity after repeated adsorption/desorption cycles, and (4) good hydrothermal and mechanical stability.[12]

Hydrotalcite-like compounds (HTlcs), also known as layered double hydroxides (LDHs) and anionic clays are bidimensional basic solids that have been used as catalysts, as adsorbents and ion exchangers for treatment of liquid wastes, and also in medicine (as antacids). The structure consists of positively charged brucite (magnesium hydroxide)-like layers with interlayer space containing charge compensating anions and water molecules.[13] The metal cations occupy the centers of octahedra whose vertexes contain hydroxide ions. The octahedra are connected by edge sharing to form an infinite sheet.[14] The general formula of the compounds is $[M^{2+}_{1-x}M^{3+}_{x}(OH)_2]A^{n-}_{x/n}$, where M^{2+} and M^{3+} are

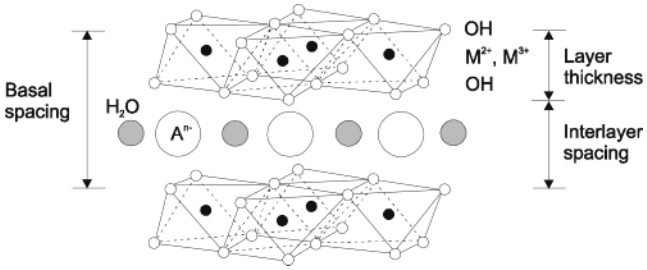

Figure 1. Structure of hydrotalcite-like compounds.

divalent (Mg^{2+}, Zn^{2+}, Ni^{2+}, etc.), and trivalent cations (Al^{3+}, Cr^{3+}, etc.), A^{n-} is a nonframework charge-compensating anion (such as CO_3^{2-}, Cl^-, SO_4^{2-}), and x is normally between 0.17 and 0.33.[13] The structure is shown in Figure 1.

Published results of CO_2 sorption on hydrotalcite-like compounds (HTlcs) suggest that sorbents in this family may be useful for CO_2 separation and capture using adsorption technologies at high temperatures.[12,15−18] The most interesting result (reported by Yong et al.[18]) is that the CO_2 adsorption capacity follows the trend $Q_{300} > Q_{20} > Q_{200}$ (where Q_T is the adsorption capacity at 1 atm and temperature T, °C). The authors suggested that this is due to a decrease of the interlayer (d) spacing between room temperature and 200 °C, resulting in less void space, which inhibits CO_2 adsorption. The authors further suggested that, at 300 °C, dehydroxylation and decarbonation of the HTlc results in structural modifications and increased porosity and an enhanced adsorption capacity for CO_2. Others have shown that promotion by alkali salts can increase both the adsorption capacity and the stability of hydrotalcite-like adsorbents.[16,17,19] Other enhancements have been described, such as small additions of rare earth elements to the hydrotalcite structure.[20] There have been numerous studies that have described the thermal decomposition of hydrotalcite and other LDHs.[21−23] In this work we have attempted to describe and quantify the decomposition and structural modifications of an HTlc in N_2, CO_2, and mixed N_2/CO_2 and to determine how those structural modifications affect the CO_2 adsorptive capacity of the HTlc.

Experimental Section

Synthesis of Hydrotalcite. The HTlc used in this work was synthesized using a coprecipitation technique. The sample was prepared as a synthetic analogue of the naturally occurring hydrotalcite mineral, $[Mg_{0.75}Al_{0.25}(OH)_2](CO_3)_{0.125}{\cdot}mH_2O$.

(4) Kikkinides, E. S.; Yang, R. T.; Cho, S. H. *Ind. Eng. Chem. Res.* **1993**, *32*, 2714.
(5) Diagne, D.; Goto, M.; Hirose, T. *Energy Convers. Mgmt*. **1995**, *36*, 431.
(6) Ishibashi, M.; Ota, H.; Akutsu, N.; Umeda, S.; Tajika, M.; Izumi, J.; Yasutake, A.; Kabata, T.; Kageyama, Y. *Energy Convers. Mgmt.* **1996**, *37*, 929.
(7) Takamura, Y.; Narita, S.; Aoki, J.; Hironaka, S.; Uchida, S. *Sep. Pur. Technol.* **2001**, *24*, 519.
(8) Gomes, V. G.; Yee, K. W. K. *Sep. Pur. Technol.* **2002**, *28*, 161.
(9) Ebner, A. D.; Ritter, J. A. *AIChE J.* **2002**, *48*, 1679.
(10) McIntyre, J. A.; Holland, C. E.; Ritter, J. A. *Ind. Eng. Chem. Res.* **2002**, *41*, 3499.
(11) IEA (International Energy Agency) *Carbon Dioxide Capture from Power Stations* (available on the Internet at http://www.ieagreen.org.uk/ sr2p.htm), 1998.
(12) Yong, Z.; Mata, V.; Rodrigues, A. E. *Sep. Pur. Technol.* **2002**, *26*, 195.
(13) Ulibarri, M. A.; Pavlovic, I.; Barriga, C.; Hermosin, M. C.; Cornejo, J. *Appl. Clay Sci.* **2001**, *18*, 17.
(14) Constantino, V. R. L.; Pinnavaia, T. J. *Inorg. Chem.* **1995**, *34*, 883.
(15) Mao, G.; Tsuji, M.; Tamaura, Y. *Clays Clay Miner.* **1993**, *41*, 731.
(16) Hufton, J. R.; Mayorga, S.; Sircar, S. *AIChE J.* **1999**, *45*, 248.
(17) Ding, Y.; Alpay, E. *Chem. Eng. Sci.* **2000**, *55*, 3461.
(18) Yong, Z.; Mata, V.; Rodrigues, A. E. *Ind. Eng. Chem. Res.* **2001**, *40*, 204.
(19) Mayorga, S. G.; Weigel, S. J.; Gaffney, T. R.; Brzozowski, J. R.; US Patent No. 6,280, 503 B1, August 28, 2001.
(20) White, M. G.; Iretskii, A. V.; Weigel, J. S.; Chiang, R. L.; Brzozowski, J. R.; International Patent No. WO2004/000440 A1, December 31, 2003.
(21) Hibino, T. Yamashita, Y.; Kosuge, K.; Tsunashima, A. *Clays Clay Miner.* **1995**, *43*, 47.
(22) Bellotto, M.; Rebours, B.; Clause, O.; Lynch, J.; Bazin, D.; Elkaïm, E. *J. Phys. Chem.* **1996**, *100*, 8535.
(23) Tichit, D.; Bennani, M. N.; Figueras, F.; Ruiz, J. R. *Langmuir* **1998**, *14*, 2086.

In the synthesis procedure, 0.75 mol of $Mg(NO_3)_2 \cdot 6H_2O$ and 0.25 mol of $Al(NO_3)_3 \cdot 9H_2O$ were dissolved in 250 mL of deionized (DI) water. The resulting solution was then added, drop-by-drop with vigorous stirring, to a 500 mL solution containing 1.7 mol of NaOH and 0.5 mol of Na_2CO_3. The resulting precipitate was then separated by vacuum filtration, washed with DI water, and dried at 100 °C in a conventional oven. The dried solid was then crushed in a mortar and pestle and stored in a glass sample bottle for subsequent characterization.

Chemical Analysis. Chemical analysis was done using X-ray fluorescence (XRF) on pellets prepared by mixing 2 g of the analyte with 2 mL (200 mg dry solids) of liquid binder to give a 32 mm diameter pellet weighing 2.2 g with a material-to-dilutent ratio of 0.1. The XRF intensities were collected on each side of the pellet using Phillips SuperQ data collection software and evaluated using Omega Data System's UniQuant 4 XRF "standardless" data analysis software. The UQ/UQ calibration was used to analyze the samples. The pellets were evaluated as oxides.

Surface Area and Porosity. The surface area (BET), meso- and microstructure, and pore size distribution (PSD) of the HTlcs were calculated from N_2 adsorption isotherms at −196 °C that were obtained using a static volumetric system (Quantachrome Autosorb-1-C). The isotherms were measured using samples that had been pretreated by heating in a vacuum at various temperatures for a minimum of 12 h. (Note: all of the samples had originally been dried at 100 °C in air). The surface area was calculated using the BET method; the mesopore volume and diameter were calculated using the density functional theory (DFT) methodology.[24] Micropore volume and diameter (width) were calculated using the Horvath−Kawazoe (H−K) equation.[24,25]

Thermal Treatment. Differential scanning calorimetry (DSC) scans were obtained using a Perkin-Elmer DS7. Thermogravimetric analysis (TGA) was done using a Perkin-Elmer TG7. Thermal decomposition products were measured using a Pfieffer Vacuum Prisma mass spectrometer during in situ heating of the sample under flowing helium in the chemisorption cell of a Quantachrome Autosorb-1C-MS.

X-ray Diffraction. High-temperature X-ray diffraction (HTXRD) patterns were collected at the High-Temperature Materials Laboratory at the Oak Ridge National Laboratory. X-ray diffraction (XRD) data were collected with a PANalytical X'Pert Pro theta−theta diffractometer using Cu Kα X-radiation. The sample stage was an Anton Paar XRK900 reactor chamber. The powder sample was packed into a macor glass−ceramic sample holder that was spun during data collection to improve the counting statistics. Two thermocouples were used to control the heating elements to provide minimal temperature gradients in the heating volume. Incident optics consisted of a 0.25° divergence slit, 0.04 rad axial divergence Soller slits, and a 0.5° antiscatter slit; receiving optics consisted of a 5 mm antiscatter slit, 0.04 rad axial divergence Soller slits, and a Ni Cu Kβ filter.

The detector was an X'Celerator real time multiple strip detector that collected data over a ~2.1° range simultaneously. All XRD data were collected with a step size of 0.0167° 2θ and a scan rate of 0.133° 2θ/s. Using the X'Celerator detector, high-quality diffraction patterns with excellent signal-to-background were collected in 4−10 min per scan.

In situ diffraction data were collected over a temperature range of 25−600 °C in flowing gases of CO_2, N_2, and a N_2/CO_2 (80/20 vol %) mixture. The gas mixture was obtained using mass flow controllers set to 80 mL N_2/min and 20 mL CO_2/min. The system was flushed with gas for several minutes before beginning the in situ XRD scans. The XRD patterns were collected from 5° to 80° 2θ; each pattern took less than 10 min to collect. XRD patterns were collected at 25 °C and then from 100 to 200 °C in 25 °C steps, from 200 to 300 °C in steps of 10 °C for the CO_2 and 80/20 mixture gases or 20 °C for the N_2 gas, from 300 to 400 °C in 10 °C steps, and finally from 400 to 600 °C in 50 °C steps. The heating rate was 20 °C/min.

CO_2 Adsorption Isotherm Measurements. High-temperature CO_2 adsorption isotherms were measured using the chemisorption cell of the Quantachrome Autosorb-1C-MS. The combined (physisorption plus chemisorption) isotherm was measured first. The sample was then evacuated, removing only the physically (weakly) adsorbed gas, and the adsorption isotherm measurement was repeated to obtain the physisorption component. The chemisorption (strong) isotherm was then determined by the difference in the combined isotherm and the physisorption (weak) isotherm. Additions of the adsorbate gas were made at volumes required to achieve a targeted set of pressures. A minimum equilibrium interval of 20 min with a tolerance of 0.5% for $P > 1$ Torr and 1.7% for $P < 1$ Torr was used to determine equilibrium for each measured point (i.e., the equilibrium criteria was checked every 20 min).

Results

Chemical Analysis. The composition of the sample was determined to be $[Mg_{0.73}Al_{0.27}(OH)_2](CO_3)_{0.135} \cdot m H_2O$ (very close to the target). The hydrotalcite structure was then confirmed by X-ray diffraction. The average weight loss after heating to 120 °C was 7.9% (assumed to be the loss of loosely held water).

Surface Area and Porosity. The adsorption capacity of an adsorbent often follows the total surface area, since there are usually more available active binding/sorption sites on a material with higher surface area. The surface and porosity of the materials after various heat pretreatments were calculated from a variety of methods using data from the adsorption of N_2 at −196 °C (i.e. in a liquid N_2 bath). The N_2 at −196 °C adsorption isotherms for the HTlc after heating to 200 and 300 °C are shown in Figure 2. Both isotherms have a similar aspect and correspond to type IV according to the IUPAC 1985 classification of physisorption isotherms. The type IV isotherm, whose initial region is closely related to the type II isotherm, tends to level off at high relative pressures.[26] Both isotherms exhibit hysteresis, which is usually associated with the filling and emptying of the mesopores by capillary condensation. The hysteresis loop for the isotherm is of the type H3, which is affected by phenomena such as delayed pore condensation, percolation, and pore blocking and also by what is known as the tensile strength effect.[27,28] The volume adsorbed was much higher for the material after dehydration at 300 °C in vacuo, indicating a higher total surface area. The adsorption isotherms for materials dehydrated at 120 and 400 °C were very similar to those that had been dehydrated at 200 and 300 °,C respectively (but are not shown for simplicity). The results for the calculated values of BET surface area and meso- and microporosity are given in Table 1. One can see that there is a significant increase in the surface area for the material after being preheated in a vacuum to 300 and 400 °C (177.4 and 183.7 m^2/g, respectively) over the same material that was heated in a vacuum to 120 and 200 °C (55.3 and 66.1 m^2/g, respectively).

(24) Quantachrome Instruments, Autosorb-1 Gas Sorption System Manual, AS-1−2, REV B, 2001.

(25) Horvath, G.; Kawazoe, K. *J. Chem. Eng. Jpn*. **1983**, *16*, 470.

(26) Rougerol, F.; Rougerol, J.; Sing, K. *Adsorption By Powders and Porous Solids*; Academic Press: London, 1999.

(27) Ravikovitch, P. I.; Neimark, A. V. *Langmuir* **2002**, *15*, 5347.

(28) Schreiber, A.; Reinhardt, S.; Finenegg, G. H. *Studies Surf. Sci. Catal.* **2002**, *144*, 177.

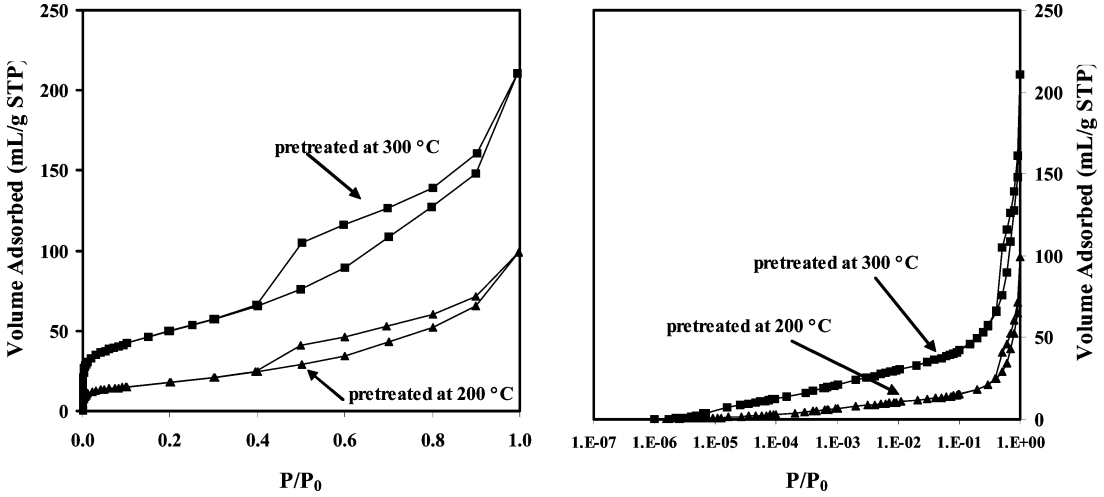

Figure 2. Adsorption of N_2 at −196 °C on hydrotalcite after thermal pretreatment at 200 °C (lower curve) and 300 °C (upper curve). The isotherms are shown on a log scale on the right to better present the low-pressure region.

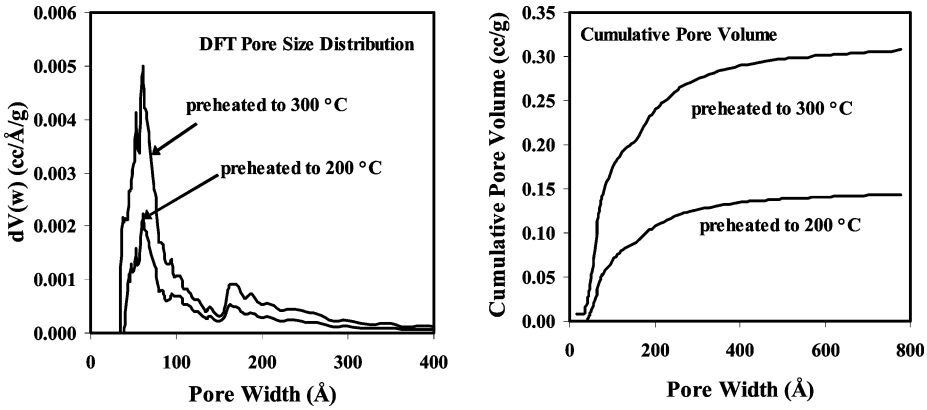

Figure 3. Mesopore size distribution (left) and cumulative mesopore volume (right) for hydrotalcite after thermal pretreatment at 200 °C (lower curve) and 300 °C (upper curve). The mesopore structures were calculated from N_2 at −196 °C adsorption isotherm data using the DFT method.

Table 1. Surface Area and Porosity of HTlc Derived from N_2 Adsorption at −196 °C after Thermal Pretreatment at the Specified Temperatures

		DFT[b]		HK[c]	
pretreatment temp,[a] °C	BET SA, m^2/g	ΣV_p, cm^3/g	D_p, Å	μD_p, Å	μV_p, cm^3/g
120	55.3	0.136	60.79	6.33	0.021
200	66.1	0.144	60.79	5.93	0.026
300	177.4	0.308	60.79	5.28	0.071
400	183.7	0.305	60.79	5.13	0.073

[a] Temperature at which the sample was heated prior to analysis; all samples were heated at the indicated temperature, in vacuo, for a minimum of 12 h. [b] Density functional theory [c] Horvath−Kawazoe equation assuming slit-type pores

Mesoporosity (Pores in the Range 20−500 Å). The mesoporosity was evaluated using the DFT method. The mesopore size distribution and cumulative mesopore volume are shown in Figure 3. The results of the analysis are given in Table 1. There is an increase in the cumulative total pore volume (as calculated by the DFT method) with increasing pretreatment temperature with a large increase between the material that had been heated to 200 and 300 °C. However, the mesopore size distribution does not change with increasing pretreatment temperature; all of the materials were calculated to have a peak pore width of approximately 61 Å.

Microporosity (Pores < 20 Å). The microporosity was evaluated using the H−K equation with slit-type pores. The micropore size distribution and cumulative micropore volume are shown in Figure 4. The results of the analysis are given in Table 1. There is an increase in the cumulative micropore volume (as calculated using the H−K equation) with increasing pretreatment temperature and, as with the mesopore volume, there is a large increase for the materials that had been heated to 300 and 400 °C. However, unlike that of the mesopore size distribution, there is a change in the peak micropore width with increasing pretreatment temperature. The material has a peak micropore size of approximately 6.33 Å after heating to 120 °C. The peak micropore size decreases more than 1 Å to approximately 5.13 Å after heating to 400 °C. The micropore size distribution, given in Figure 4, shows the peak in the 5−6.5 Å range and a second smaller peak in the 8−10 Å range (consistent with the D−R plot prediction of multiple types of micropores).

Thermal Decomposition. To understand the structural effects on CO_2 adsorption, it is important to understand the dehydration and decarbonation of the material. This was done in a series of experiments. First, the decomposition products were measured by heating the material from room temperature to 900 °C in a chemisorption analysis cell of a Quantachrome

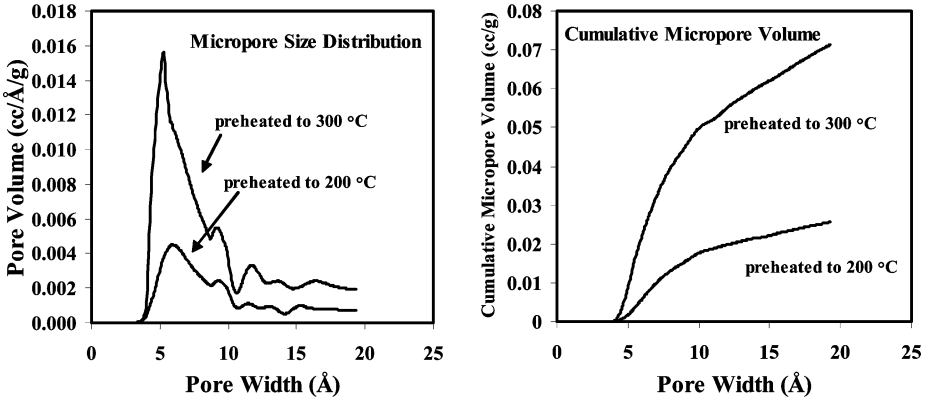

Figure 4. Micropore size distribution (left) and cumulative micropore volume (right) for hydrotalcite after thermal pretreatment at 200 °C (lower curve) and 300 °C (upper curve). The mesopore structures were calculated from N_2 at −196 °C adsorption isotherm data using the H−K method (assuming slit-type pores).

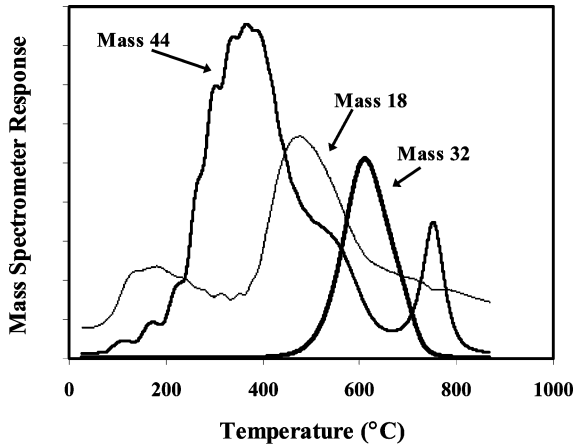

Figure 5. Mass spectrometer response for evolved gases upon heating of the HTlc at 20 °C/min in flowing He.

Autosorb-1-C with mass spectrometer attachment. The sample (approximately 1 g) was first used to collect adsorption isotherm data for sorption of CO_2 at 300 °C. The sample was then cooled to room temperature and then heated at 20 °C/min in flowing He. A plot of the mass spectrometer response to the effluent gas concentration versus temperature is shown in Figure 5. Note that there appears to be some moisture in the He carrier gas.

Most of the loosely held water (mass 18) in the interlayer space is lost before the material is heated to 300 °C, with the majority being evolved in the 120−180 °C range. There is some initial decarbonation starting at about 100 °C, but the CO_2 evolution (mass 44) does not increase significantly until the material is heated to >200 °C. The CO_2 evolution peaked at about 360 °C. At about that same temperature, an evolution of mass 18 begins, peaking at about 470 °C before decreasing. This is likely the result of the disappearance of OH^- groups (dehydroxylation), likely in the Al−OH−Mg configuration. As the material further decomposes, there is a sharp evolution of O_2 (mass 32) that peaks at about 620 °C and a second peak of CO_2 evolution peaking at about 760 °C. These are the result of the complete decomposition of the material to a solid solution of MgO and Al_2O_3. Hibino et al.[21] observed that 20−30% of carbonates remain after heating the Mg−Al−CO_3 HTlc (with Al/(Al + Mg) = 0.33) to 500 °C, and they are released between 600 and 900 °C as Al^{3+} migrates into MgO to form spinel ($MgAl_2O_4$).

In separate experiments, approximately 10 mg of the HTlc material was placed in the TG7 sample dish. The samples were then heated at 5 °C/min in flowing N_2 and CO_2. Separately approximately 20 mg of the material was placed in the DS7 sample holder and the samples were heated at 20 °C/min in flowing N_2 and CO_2. The TGA profiles for the sample in N_2 and CO_2 are shown in Figure 6 (left). One can see that in both cases there is a sharp immediate decrease in weight of approximately 15% in the temperature range of 30−250 °C.

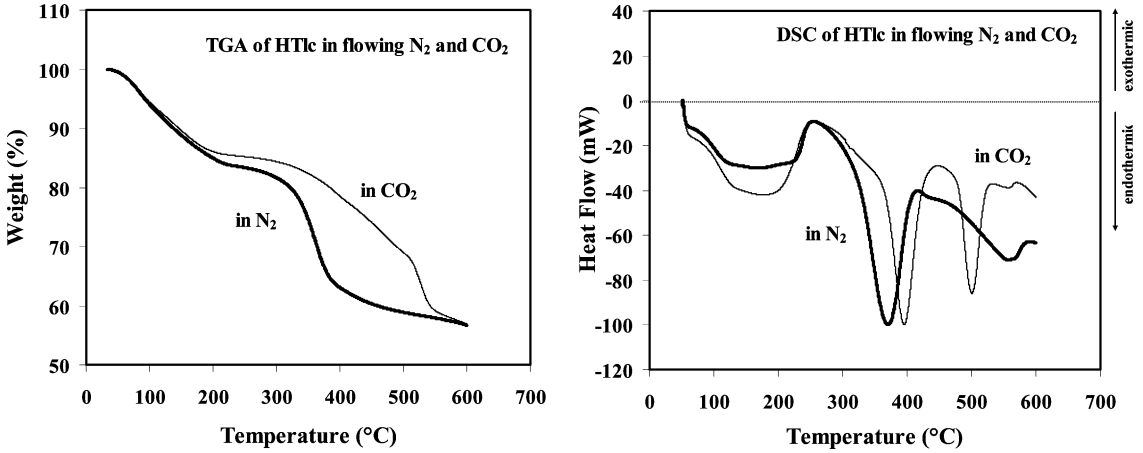

Figure 6. Thermogravimetric analysis of HTlc in flowing N_2 and CO_2 with a heating rate of 5 °C/min and DSC profile for HTlc in flowing N_2 and CO_2 with a heating rate of 20 °C/min.

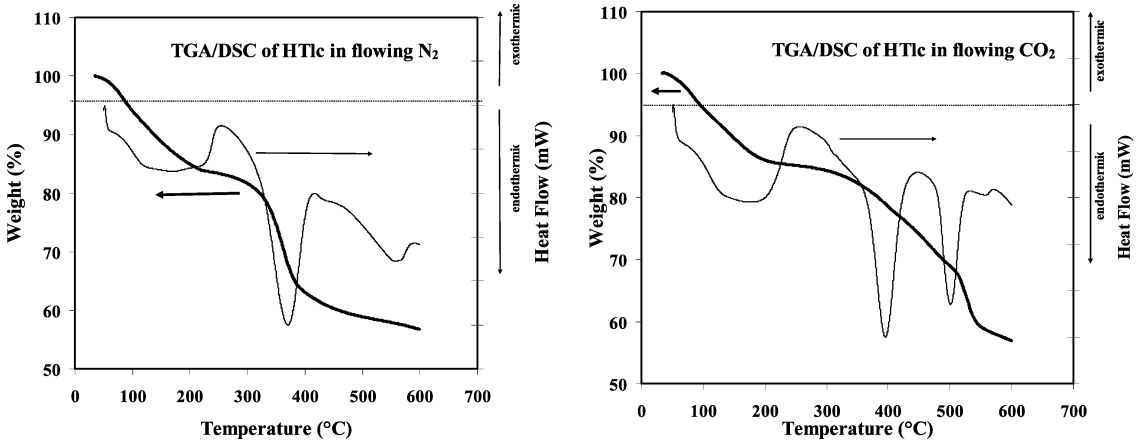

Figure 7. TGA/DSC scans for HTlc in flowing N_2 (left) and in flowing CO_2 (right). The heating rates were 5 °C/min for the TGA profiles and 20 °C/min for the DSC profiles.

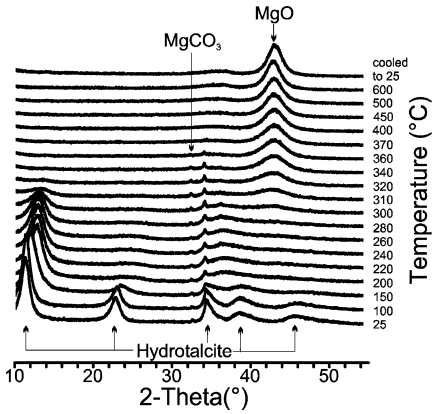

Figure 8. In situ HTXRD patterns for the HTlc in flowing N_2 as a function of temperature.

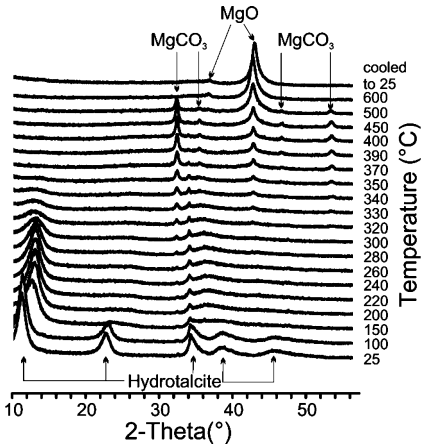

Figure 9. In situ HTXRD patterns for the HTlc in flowing CO_2 as a function of temperature.

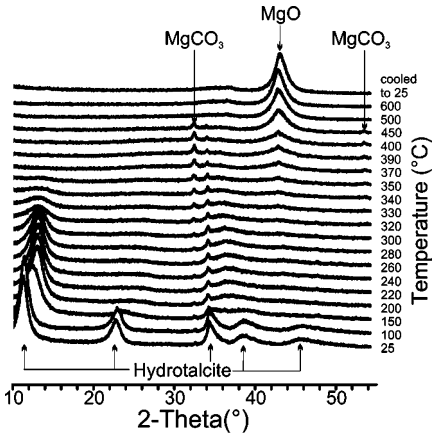

Figure 10. In situ HTXRD patterns for the HTlc in a flowing mixture of N_2/CO_2 (80/20) as a function of temperature.

This is almost entirely due to loss of loosely held water in the interlayer space and some initial decarbonation. The sample that was heated in flowing N_2 then shows another sharp decrease in weight in the temperature range of 300−400 °C. This is due to a significant decarbonation through the loss of the interlayer charge compensating carbonate anion (as evolved CO_2). The sample that was heated in flowing CO_2 also shows this weight loss due to thermal decarbonation. However, the weight loss is not as abrupt due to concomitant CO_2 physisorption and mineralization of the sample. There is another sharp decrease in the sample weight at about 550 °C that is likely due to decomposition of the mineralized $MgCO_3$.

Figure 6 (right) also shows the DSC scans for the material under the same conditions. The materials, under both the N_2 and CO_2 atmospheres, showed broad initial curves in the range of water removal (room temperature to 250 °C). A large peak immediately followed, corresponding to CO_2 evolution as the result of decarbonation of the interlayer charge compensating carbonate anion. The peak was at approximately 360 °C for the material in flowing N_2 and approximately 390 °C for the material in flowing CO_2. For the material that was heated in flowing CO_2, there is a second exothermic peak at about 500 °C, which is assumed to be from $MgCO_3$ decomposition. Both materials then show a peak at about 550−570 °C, which is assumed to be evolution of O_2 as the structure is initially being broken down to a solid solution. For comparison, the TGA/DSC curves are shown again in Figure 7 with the curves in N_2 shown on the left and in CO_2 on the right.

X-ray Diffraction. To further characterize structural changes that may affect CO_2 adsorption on HTlc, HTXRD patterns were collected under varying conditions. The diffraction patterns are shown in Figures 8 (in N_2), 9 (in CO_2), and 10 (in N_2/CO_2 mixture). The peak shift, most readily observed with the d_{003} peak in each figure, was due to three mechanisms: the thermal expansion of the unit cell, sample displacement as the bulk sample shrank due to desorption of water, and

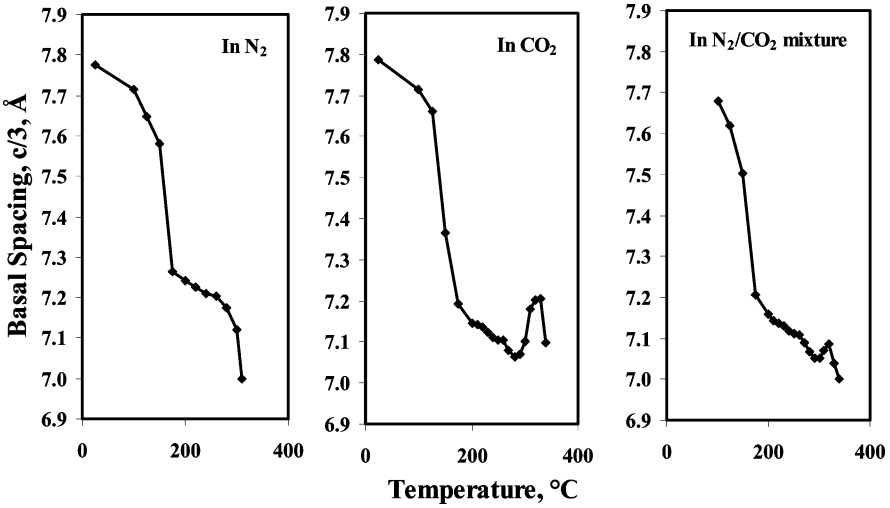

Figure 11. Basal spacing (c/3) versus temperature from in situ XRD of HTlc in N_2, CO_2, and an N_2/CO_2 (80/20) mixture.

collapse of the interlayer spacing as water desorbed. To measure the change in the interlayer spacing, the positions of the (003) and (006) peaks were determined at each temperature using a profile fitting routine. By using both diffraction peaks, the effects of sample displacement were deconvoluted from the changes in the c lattice parameter so that the c lattice parameter could be accurately calculated. The unit cell used for HTlc consisted of three basal layers stacked along the c-direction; therefore, the basal layer thickness was one-third of the c lattice parameter. The resulting plot of the basal layer thickness as it changed with temperature is shown in Figure 11. The basal spacing decreased from approximately 7.8 to 7.2 Å when the HTlc was heated from room temperature to 200 °C in any of the tested atmospheres. In N_2, the basal spacing decreased to 7.1 Å when heated to 300 °C and reached a minimum spacing of 7.0 Å before the HTlc peaks became unobservable at >310 °C. When the HTlc was heated in CO_2 or in the N_2/CO_2 (80/20) mix, the basal layer thickness decreased to 7.0 Å at 290 °C. The HTlc peaks persisted up to 340 °C; however, from 300 to 330 °C the basal layer actually increased from 7.0 to 7.2 Å in the CO_2 and 7.1 Å in the N_2/CO_2 mix. Above 330 °C, the basal layer then decreased to 7.1 Å in CO_2 and 7.0 Å in the N_2/CO_2 mix before the d_{003} peak disappeared above 340 °C. The HTlc behaved very similarly up to 300 °C in the CO_2 and N_2/ CO_2 mix; however, above 300 °C the basal layer "swelled" more in CO_2. Assuming that the thickness of one layer of the HTlc is 4.8 Å, as has been previously reported,[29] then the interlayer spacing therefore decreased from 3.0 to 2.4 Å after heating from room temperature to 200 °C and then to ~2.2 Å after further heating to 300 °C. After the material is heated beyond 300−340 °C, the well-defined layered structure is lost and the material becomes nearly amorphous. The structural nature of the material upon heating to higher temperatures is dependent on the environment in which it is heated. The slight swelling of the basal spacing just before the structure collapses (for the CO_2 and N_2/CO_2 samples) is likely due to adsorption of CO_2 in the interlayer space.

XRD in N_2. The HTlc that was heated in the flowing N_2 (Figure 8) showed very small peaks at ~32° (2θ) that were identified as $MgCO_3$. These peaks were present at room temperature and disappeared by 360 °C. This indicates that there was some small amount of $MgCO_3$ initially present in the HTlc sample. In the Mg−Al−CO_3 HTlc structure the CO_3^{2-} anion has very weak, if any, direct interaction with the Mg^{2+} and Al^{3+} structural cations.[30] A broad peak at ~43° (2θ), indicating the presence of MgO, becomes noticeable at 300 °C and continues to grow with heating.

XRD in CO_2. The diffraction patterns for the HTlc when heated in flowing CO_2 are shown in Figure 9. The patterns are similar to those in flowing N_2 in that the low-angle d_{003} peaks shift to the right with heating (as mentioned earlier). However, the $MgCO_3$ peak at 33° (2θ) continues to grow, indicating mineralization of the HTlc with increasing temperature in the flowing CO_2. The peak then disappeared between 500 and 600 °C, indicating decomposition of the $MgCO_3$ (though in the thermal decomposition experiment described earlier, a second CO_2 peak, which was ascribed to $MgCO_3$ decomposition, was not seen until the sample had been heated to greater than 700 °C. As with the material that was heated in N_2, a peak at ~43° (2θ) begins to form when heating above 300 °C. However, the MgO peaks, when compared to those of the HTlc in flowing N_2, are much sharper and well defined.

XRD in N_2/CO_2 Mixture. Figure 10 shows the in situ HTXRD patterns for the HTlc in a flowing mixture of N_2/CO_2 (80/20 vol %) as a function of temperature. The diffraction patterns seem to have commonality with both the previously described conditions. The familiar $MgCO_3$ peak at 33° (2θ) is again seen in this sample; however, the intensity does not grow with temperature, as was obvious with the material that was heated in flowing CO_2. The peak had then disappeared from the patterns collected at 500 °C, earlier than that in flowing CO_2. As with the previous samples, the MgO peak at ~43° (2θ) begins to form when heating above 300 °C. However, these peaks seem much sharper and better defined than those of the patterns collected in flowing N_2, but not as sharp and clearly defined as those collected in flowing CO_2. In general, the MgO peaks are sharper in the flowing CO_2, wider in the flowing N_2, and between

(29) Calvini, F.; Trifiro, E.; Vaccari, A. *Catal. Today* **1991**, *11*, 173.

(30) Yang, W.; Kim, Y.; Liu, P. K. T.; Sahimi, M.; Tsotsis, T. T. *Chem. Eng. Sci.* **2002**, *57*, 2945.

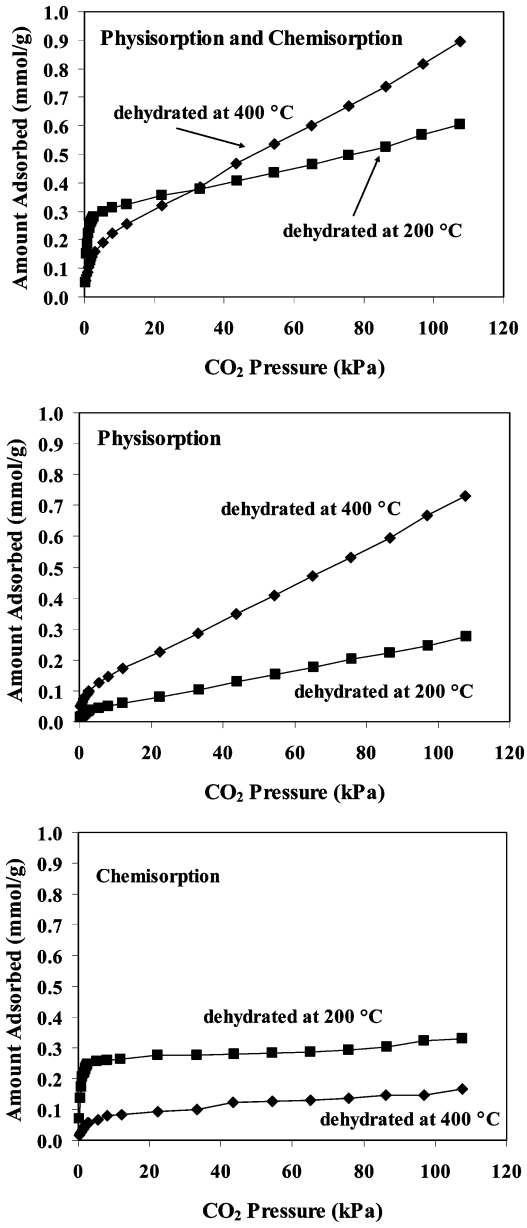

Figure 12. Adsorption isotherms for CO_2 adsorption on HTlc at 200 °C after the material had been preheated in vacuo at 200 and 400 °C (as indicated on the plots). The combined isotherm (physisorption + chemisorption, shown in the top plot) was measured first. The sample chamber was then evacuated under vacuum to desorb the physisorbed component and the isotherm measurement was repeated for the physisorption component (shown in the middle plot). The chemisorbed portion (shown in bottom plot) was determined via difference between the initial (combined) and second (physisorption) isotherms.

for the N_2/CO_2 mixture. All of the peaks are broader than the instrumental profile, indicating that there is a sample effect that is causing the peaks to broaden. This can be caused by crystallite size, indicating that larger MgO crystallites are grown in CO_2 than in N_2 (and somewhere between for the N_2/CO_2 mixture). This will be explored in continued studies with this hydrotalcite material.

Adsorption of CO_2. The focus of this work was to determine how thermally induced structural changes in the HTlc affect the adsorption of CO_2 at high temperatures. In most of our experiments, CO_2 adsorption

Table 2. Physisorption Capacities (at 200 °C and 107 kPa) Normalized to Total Surface Area and Pore Volume for HTlc after Heating to 200 and 400 °C in Vacuum

	BET SA,	pore vol,	physisorption		
sample	m^2/g	cm^3/g	mmol/g	μmol/m^2	mmol/cm^3
HTlc-200	66.1	0.144	0.274	4.145	1.903
HTlc-400	183.7	0.305	0.731	3.979	2.397

isotherms are measured at temperatures between 300 and 400 °C. However, in an effort to capture structural effects, in this work adsorption isotherms were measured at 200 °C. Samples of the HTlc were first preheated in a vacuum to 200 and 400 °C. As shown earlier, there is a significant difference in the pore volume and total surface area for samples that have been heated to 200 and 400 °C. The combined (physisorption plus chemisorption) isotherm was measured first and the sample was then evacuated, removing only the physically (weakly) adsorbed gas. The adsorption isotherm measurement was then repeated to obtain the physisorption component. The chemisorption (strong) isotherm was then determined by the difference in the combined isotherm and the physisorption (weak) isotherm. The isotherms for CO_2 adsorption at 200 °C are shown in Figure 12. The combined isotherms are shown in the top plot. The isotherms differ in that the material that was heated to 200 °C (HTlc-200) shows a high adsorption at low CO_2 pressures before stabilizing to a moderate increase in adsorption with increasing pressure. The sample that was heated to 400 °C (HTlc-400) shows less adsorption at lower CO_2 pressures with a less pronounced "knee" in the isotherm. The amount of CO_2 adsorbed then increases with increasing pressure with a capacity of ~0.9 mmol CO_2/g of sorbent at 107 kPa pressure. The capacity of the HTlc-200 sample was ~0.6 mmol/g at 107 kPa pressure. To understand this we look at the physisorption and chemisorption contributions.

Physisorption. The physisorption isotherms are given in Figure 12 (middle plot). Both isotherms have a similar aspect, but the HTlc-400 sample has a greater capacity. From the look of the HTlc-400 isotherm, it does appear that this is some additional chemisorption contribution. This is consistent with previous observations of an irreversible decline in the adsorption capacity with cycling.[17] But most of the increase in physisorption capacity for the HTlc-400 sample is easily explained by the increase in total surface area and pore volume upon heating to temperatures greater than 300 °C. Table 2 shows the absolute CO_2 physisorption capacity for both samples (HTlc-200 and HTlc-400 at 200 °C and 107 kPa) and the physisorption normalized to total surface area and the total pore volume. When normalized to the total surface area and total pore volume, the physisorption amount is approximately the same for both samples.

Chemisorption. The chemisorption isotherms are given in Figure 12 (bottom plot). The isotherms look very similar with sharp initial adsorption at low CO_2 pressures before reaching a saturation point, where the isotherm is nearly flat with increasing pressure. However, contrary to the physisorption capacities, the sample that had been preheated to 200 °C had the greater chemisorption capacity (~0.33 mmol/g versus ~0.17 mmol/g at 200 °C and 107 kPa). The combined chemisorption and chemisorption capacities (at 200 °C

Table 3. Adsorption Capacities (at 200 °C and 107 kPa) for HTlc after Heating to 200 and 400 °C in Vacuum

sample	CO_2 adsorption capacity, mmol/g			% chemisorption contribution
	combined	physisorption	chemisorption	
HTlc-200	0.604	0.274	0.330	54.6%
HTlc-400	0.896	0.731	0.165	18.4%

and 107 kPa) for both samples are given in Table 3. The percent of the chemisorption contribution to the total capacity is also given in Table 3. More than half (54.6%) of the total CO_2 adsorption capacity for the HTlc-200 sample came from the chemisorption contribution, which represented less than 20% of the total capacity for the HTlc-400 sample.

Discussion of Results. The high-temperature adsorption of CO_2 on Mg−Al−CO_3 hydrotalcite-like compound is affected by structural changes that take place upon heating of the material. Upon heating to 200 °C, most of the loosely held water is lost but most of the CO_3^{2-} is still present. The material retains its layered structure, but the interlayer spacing is collapsed due to the loss of the water, and the space is decreased by ~0.3 Å. However, there is no significant increase in total surface area or total pore volume, and physisorption of CO_2 at 200 °C (and lower) is limited as a result. Chemisorption of CO_2 at high temperatures is likely due exclusively to mineralization of the sample by the reaction of Mg and CO_2 to form $MgCO_3$. This is seen in the high-temperature XRD patterns for samples in flowing CO_2 and in the N_2/CO_2 mixture. The charge-compensating carbonate anion in the interlayer spacing does not interact directly with framework Mg^{2+}. However, the sample that had been heated to 200 °C must have had increased availability of the Mg^{2+} cation, since the chemisorption is higher than for the sample that had been heated to 400 °C and represents a higher percentage contribution to the total combined adsorption capacity. Constantino and Pinnavaia[14] studied the relationship between the composition and structure of various Mg−Al layered double hydroxides on catalytic activity. They found that the crystalline LDH intercalates (activated below the temperature of structural collapse) were more reactive for base-catalyzed reactions than the amorphous oxides formed by thermal decomposition of the LDH structures. Tichit et al.[23] reported a progressive increase in the lattice *a* parameter as with increasing temperature and progressive collapse of the layered structure. They attribute this to migration of Al^{2+} (whose ionic radius is slightly lower than that of Mg^{2+}) from the framework octahedral brucite-type layers to tetrahedral sites in the interlayer. Bellatto et al.[22] have estimated this to be 10% (at a minimum) of the Al^{3+} at 200 °C. This effectively makes the framework Mg^{2+} ions more available for reaction with CO_2. The Mg^{2+} ions are then less available in samples that have been heated to above ~300 °C, where the layered structure collapses and the material becomes amorphous. Upon heating to 400 °C the CO_3^{2-} in the interlayer is decomposed and the material is completely dehydrated and partly dehydroxylated. It is at this point that a three-dimensional network is formed. Bellato et al.[22] suggested that the 3-D network poses constraints on the octahedral layers, which contract along the plane. An increase in surface area occurs along with the contraction of the octahedral layer. The 3-D structure consists of a close-packed oxygen network, which traps in its interstices a disordered cation configuration with octahedral (M^{2+}) and tetrahedral (M^{3+}) cations. The increased surface area and pore volume and the decreased availability of the Mg^{2+} cation favor physisorption over chemisorption for these samples.

The hydrotalcite-like compounds are very open to physical and chemical manipulation. There are numerous combinations of M^{3+} and M^{2+} cations and interlayer charge-compensating anions that can be used to create HTlcs with unique properties. The structure and properties of the materials are affected by the thermal history as well. With the proper understanding of these structure−property relationships, HTlc may conceivably be synthesized and tailored for use in a CO_2 separation and capture technology, such as pressure swing adsorption (PSA).

Acknowledgment. Jon Gregory, an undergraduate engineering student at North Carolina State University, performed the TGA/DSC analyses with assistance from Rob Keeney of ARCADIS G&M (Durham, NC). Kara Linna, a NRMRL/EPA postdoctoral fellow, performed the XRF analyses. The HTXRD portion of this work was sponsored by the Assistant Secretary for Energy Efficiency and Renewable Energy, Office of FreedomCAR and Vehicle Technologies, as part of the High-Temperature Materials Laboratory User Program. Oak Ridge National Laboratory is managed by UT-Battelle, LLC for the U.S. Department of Energy under contract number DE-AC05−00OR22725.

CM040060U